

PAPER • OPEN ACCESS

Two-dimensional oxygen functionalized honeycomb and zigzag dumbbell silicene with robust Dirac cones

To cite this article: Xin Chen *et al* 2021 *New J. Phys.* **23** 023007

View the [article online](#) for updates and enhancements.



PAPER

Two-dimensional oxygen functionalized honeycomb and zigzag dumbbell silicene with robust Dirac cones

OPEN ACCESS

RECEIVED

17 November 2020

REVISED

3 January 2021

ACCEPTED FOR PUBLICATION

13 January 2021

PUBLISHED

8 February 2021

Original content from
this work may be used
under the terms of the
[Creative Commons
Attribution 4.0 licence](#).

Any further distribution
of this work must
maintain attribution to
the author(s) and the
title of the work, journal
citation and DOI.

Xin Chen¹ , Linyang Li^{2,3,*} , François M Peeters^{3,4}  and Biplab Sanyal^{1,*} ¹ Department of Physics and Astronomy, Uppsala University, Box 516, 751 20 Uppsala, Sweden² School of Science, Hebei University of Technology, Tianjin 300401, People's Republic of China³ Department of Physics, University of Antwerp, Groenenborgerlaan 171, B-2020 Antwerp, Belgium⁴ Department of Physics and Astronomy, Key Laboratory of Quantum Information of Yunnan Province, Yunnan University, Kunming 650091, People's Republic of China

* Author to whom any correspondence should be addressed.

E-mail: linyang.li@hebut.edu.cn and biplab.sanyal@physics.uu.se**Keywords:** 2D materials, density functional theory, dumbbell silicene, Dirac semimetal, topological insulator, functionalizationSupplementary material for this article is available [online](#)

Abstract

Dumbbell-like structures are recently found to be energetically favored in group IV two-dimensional (2D) materials, exhibiting rich physics and many interesting properties. In this paper, using first-principles calculations, we have investigated the oxidized form of the hexagonal honeycomb (ODB-h) and zigzag dumbbell silicene (ODB-z). We confirm that both oxidation processes are energetically favorable, and their phonon spectra further demonstrate the dynamic stability. Contrary to the pristine dumbbell silicene structures (PDB-h and PDB-z silicene), these oxidized products ODB-h and ODB-z silicene are both semimetals with Dirac cones at the Fermi level. The Dirac cones of ODB-h and ODB-z silicene are at the *K* point and between *Y* and Γ points respectively, possessing high Fermi velocities of $3.1 \times 10^5 \text{ m s}^{-1}$ (ODB-h) and $2.9\text{--}3.4 \times 10^5 \text{ m s}^{-1}$ (ODB-z). The origin of the Dirac cones is further explained by tight-binding models. The semimetallic properties of ODB-h and ODB-z are sensitive to compression due to the self-absorption effect, but quite robust against the tensile strain. These outstanding properties make oxidized dumbbell silicene a promising material for quantum computing and high-speed electronic devices.

1. Introduction

Inspired by the great success of graphene [1–3], related research has been conducted to search for monolayer mode of the same group elements. Monolayer 2D sheets of silicon, germanium, and tin, namely silicene, germanene, and stanene, have been predicted to be stable and also have recently been achieved by epitaxial growth on substrates [4–6]. A lot of attention has been paid to silicene [7–14] due to its relevance to silicon-based microelectronic industry. Unlike graphene, free-standing silicene has a low-buckled (LB) single-layer structure due to the pseudo-Jahn–Teller effect [15]. The resulting dangling bond makes silicene easily chemically functionalized by many kinds of adsorbed atoms or functional groups [16, 17], such as hydrogen [18–20], halogens [21], alkali earth, transition metals [22], oxygen [23, 24] and CH_3 groups [25]. Recently, it was shown that by adsorbing Si atoms, silicene reconstructs and form dumbbell-like (DB) units [26, 27]. These DB units significantly stabilize the structure, and a series of DB silicene structures was proposed based on such DB units.

Pristine DB silicene with dumbbell units arranged in a honeycomb pattern (PDB-h) was reported to be a strain-induced quantum spin Hall (QSH) insulator [28]. Also, its allotrope with DB units arranged in a zigzag pattern (PDB-z) was demonstrated to have the lowest energy of all dumbbell silicene structures [29]. Furthermore, with the dangling bonds passivated by hydrogen atoms or by some organic clusters, functionalized DB structures have been reported to be stable and exhibiting interesting electronic

properties, which has dramatically extended its possible applications [30–32]. However, in contrast to pristine and hydrogenated structures, studies of oxidization are scarce, while oxidization is very important for the application of silicon-based materials [24].

Using density functional theory (DFT), we demonstrate that O atoms can be chemically bonded to these silicon atoms on top site of PDB-h and PDB-z, leading to oxidized dumbbell silicene (labeled as ODB-h and ODB-z respectively), which have geometries similar to hydrogenated DB stanene [30]. We have investigated the structural and electronic properties along with the energetics of ODB-h and ODB-z and demonstrated their energetic and dynamic stability. More interestingly, both types of oxidized dumbbell silicene possess Dirac cones at the Fermi level. In ODB-h, Dirac cones are at the high-symmetry K point with a high Fermi velocity of $3.1 \times 10^5 \text{ m s}^{-1}$. In ODB-z, Dirac cones are situated on the line between Y point and Γ point in the Brillouin zone, with an anisotropic Fermi velocity of $2.9\text{--}3.4 \times 10^5 \text{ m s}^{-1}$. The analysis of the atomic orbital projected density of states (PDOS) and electron wavefunctions of the Dirac cones shows that in ODB-h and ODB-z, the p_z orbitals of Si(α) and even more than $p_{x,y}$ orbitals of oxygen atoms dominantly contribute to the Dirac cones. This conclusion is further confirmed by our tight-binding models containing only the $p_{x,y}$ orbitals of O atoms, which well reproduces the PBE electronic band structures near the Fermi level. Moreover, we have investigated the effect of external strain on the electronic properties of ODB-h and ODB-z and found that the semi-metal property is robust against tensile strain. Finally, with the spin-orbital coupling (SOC) effect taken into account, nontrivial bandgaps of roughly 20 meV are opened, which shows that ODB-h and ODB-z are both topological insulators.

2. Computational details

All the calculations were performed employing the projector augmented wave (PAW) [33, 34] based density functional code VASP [35, 36]. The generalized gradient approximation in the form of Perdew, Burke, and Ernzerhof [37] (PBE) was used for the exchange-correlation potential. The energy cutoff of the plane waves was set to 600 eV. The energy precision of 10^{-5} eV was used for the convergence. The effect of vertical interaction was avoided by taking a vacuum of more than 20 Å. The structures were optimized using the conjugate gradient algorithm (CG) until the maximum Hellmann-Feynman force on each atom becomes smaller than 0.01 eV Å^{-1} . The Brillouin zone (BZ) was sampled by using $11 \times 11 \times 1$ Monkhorst–Pack grid. SOC was included in the Hamiltonian [38]. The phonon spectra were calculated using a frozen phonon approach [39] within the PHONOPY code [40].

The binding energies of O atom to DB silicene are calculated by

$$E_{\text{bind}} = \frac{1}{4}[E(\text{ODB}) - 4E(\text{O}) - E(\text{PDB})], \quad (1)$$

where $E(\text{ODB})$ and $E(\text{PDB})$ denote the energies of honeycomb or zigzag ODB silicene, and PDB silicene, $E(\text{O})$ denotes the energy of one isolated oxygen atom.

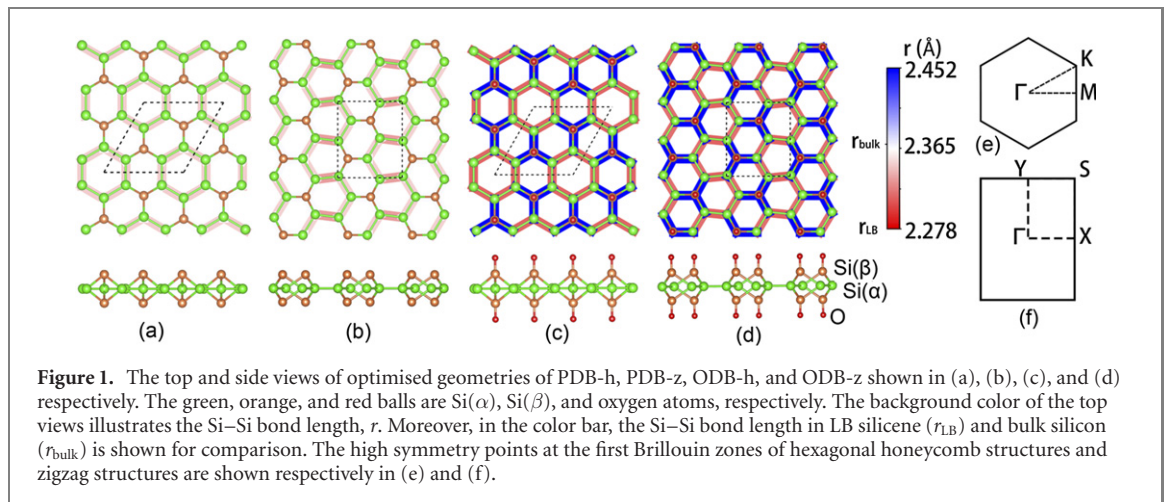
As the electronic bandgap in PBE calculation is underestimated, we have also used the Heyd–Scuseria–Ernzerhof (HSE) hybrid functional in the framework of HSE06 [41]. The energy cutoff of the plane waves is the same as for the PBE calculation, and the BZ was sampled by using $15 \times 15 \times 1$ Gamma centered Monkhorst–Pack grid.

3. Results

3.1. Optimized geometries

The optimized geometry of PDB-h silicene monolayer is shown in figure 1(a). In this configuration, the Si atoms can be divided into two types, fourfold coordinated Si(α) atoms, similar to Si atoms in a bulk crystal, and threefold coordinated Si(β) atoms, similar to atoms in LB silicene. Every three Si(α) and two Si(β) atoms form one cage-like unit, and the cage-like units are arranged in a hexagonal honeycomb pattern. Our calculated lattice constant is 7.43 Å, which is in good agreement with reference [26]. The thickness of the configuration given by the distance between up-plane and down-plane Si(β) atoms is 2.71 Å.

With all three-fold silicon atoms bonded with oxygen atoms, we get the ODB-h structure, as shown in figure 1(c). In ODB-h, not only Si(α) but also Si(β) atoms are fully coordinated. The Si–O bond length is 1.55 Å, roughly the same as that in β -cristobalite [42], and smaller than that of Si–O bond in α -quartz (1.61 Å). The lattice constant is increased to 7.49 Å, with a longer distance of 4.32 Å between two same-plane Si(β). The thickness of the monolayer characterized by the distance between up-plane and down-plane O atoms increases to 5.92 Å, in which the distance between up-plane and down-plane Si(β) atoms increases to 2.82 Å, implying stronger sp^3 hybridization in Si(β).



By *ab initio* structure-prediction calculations using a constrained crystal-structure prediction algorithm, Borlido *et al.* predicted that a zigzag like DB silicene has the lowest energy among all DB silicene structures [29]. As shown in figure 1(b), PDB-z silicene is also realized with cage-like units, but the units are arranged in a zigzag pattern. According to our PBE functional calculations, the primitive cell is a rectangle, with its lattice parameter being 6.40 Å and 7.42 Å, and the area being 4.75 Å²/atom, almost the same as in PDB-h, i.e. 4.78 Å²/atom.

The oxidized form, ODB-z silicene is shown in figure 1(d). With a similar rectangular unit cell, the lattice constants are enlarged to 6.47 Å and 7.48 Å. The distance between two Si(β) layers is 2.83 Å, and the Si-O bond length is 1.55 Å, both of which are very close to that in ODB-h, implying similar hybridization mechanism in ODB-z and ODB-h silicene.

The Si-Si bond lengths are illustrated by the background colors in figures 1(a)–(d). In all the PDB and ODB structures, the bonds between two Si(α) atoms (labelled as $r_{\alpha,\alpha}$) are shorter than 2.365 Å, showing red colors, and the bonds between Si(α) and Si(β) atoms (labelled as $r_{\alpha,\beta}$) are longer than $r_{\alpha,\alpha}$, showing white or blue colors. Comparing the Si-Si bond lengths in pristine DB silicene and oxidized DB silicene, oxidation significantly changes the Si-Si bonds. In PDB structures, $r_{\alpha,\alpha}$ and $r_{\alpha,\beta}$ are quite close to the Si-Si bond length in bulk silicon (r_{bulk}). In contrast, in ODB structures, the two lengths are very different. By oxidation, $r_{\alpha,\alpha}$ is shortened to roughly 2.28 Å, close to the Si-Si bond length in LB silicene (r_{LB}), while $r_{\alpha,\beta}$ are increased to about 2.45 Å.

3.2. Chemical bonding and structural stability

To compare the bonding nature in PDB-h, PDB-z, ODB-h, and ODB-z, electron localization functions (ELF) are calculated and analyzed. To highlight the bonds between Si(α), Si(β) atoms, and between Si(β) and O atoms, we plot the sliced ELF contour map in the top panel of figure 2. The region with an ELF value of 1 indicates fully localized electrons, the region close to 0 is typical of a low electron density area, and the region of 0.5 is an area with a homogeneous electron gas. Interestingly, the ELF contour plots of ODB-h and ODB-z are quite similar, which implies that the bonding mechanism of ODB-h and ODB-z have no significant difference. Comparing PDB and ODB monolayers, it is found that with O atoms adsorbed, the localization of electrons inside the DB silicene layers is weakened. Compared to PDB, electrons between Si(α) and Si(β) in ODB silicene are less localised. Furthermore, in ODB, the electrons around O atoms behave mainly as a homogeneous electron gas. The binding energy of O atoms in PDB-h and PDB-z silicene is, respectively, −5.19 eV/O atom and −5.17 eV/O atom, implying that O atoms are chemisorbed on pristine DB-h and DB-z.

Contrary to carbon atoms, silicon atoms prefer to be fourfold co-ordinated compared to threefold co-ordination. This is seen from the relatively higher stability of pristine DB-h and DB-z compared to LB silicene. With dangling bonds filled by O atoms, the stability of ODB-h and ODB-z is quite promising. We will investigate the stability by their energetic preference, which is measured by their formation energy, and through their dynamical stability, which is confirmed by their phonon spectra.

The formation energy of oxidized DB silicene can be hinted at by the reaction: $\text{Si}_{10} + \text{O}_2 \rightarrow \text{Si}_{10}\text{O}_4$, in which Si_{10} denotes PDB silicene, O_2 is oxygen gas, and Si_{10}O_4 is ODB silicene. The negative formation energy (−0.675 eV/atom for ODB-h and −0.667 eV/atom for ODB-z) implies that the reaction is exothermic. We further confirmed their dynamic stability by the phonon spectra calculated along the high symmetry directions in the first BZ, as shown in figure 2 of the bottom panel. It is observed that the

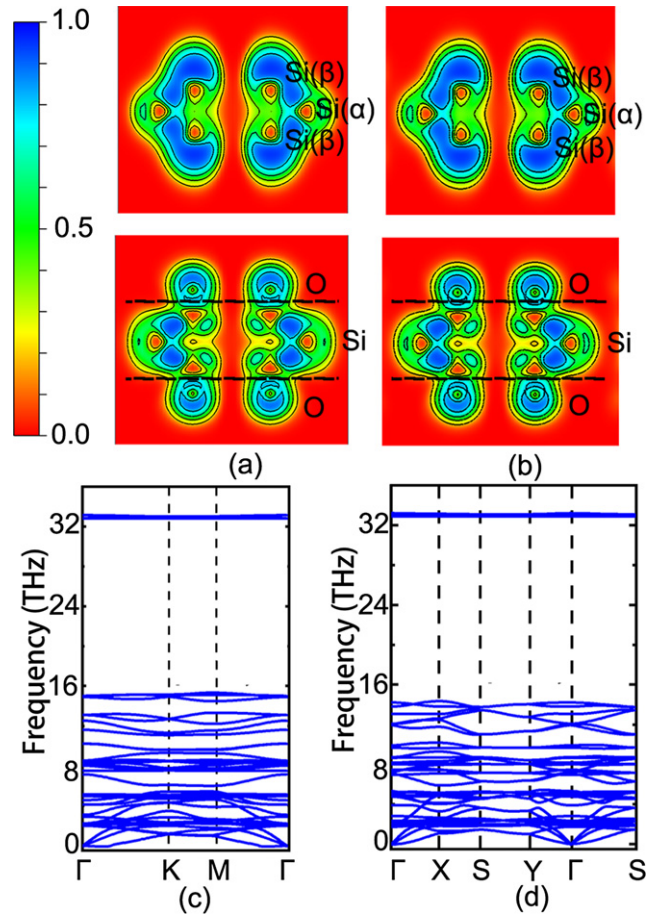


Figure 2. The top panel is the (x, y) -plane slice view of the ELF of PDB-h and ODB-h (a), PDB-z, and ODB-z (b). The bottom panel is the phonon spectrum of ODB-h (c), and ODB-z (d), respectively.

phonon spectra of ODB-h and ODB-z are quite similar in the low energy part. In both cases, the optical phonon modes have a gap at around 6 THz, and most of their optical phonon modes below 7 THz are concentrated around 3.5 THz and 5 THz. There are several high energy modes (of about 34 THz) in both structures, whose eigenvectors are shown in the supplementary files (<https://stacks.iop.org/NJP/23/023007/mmedia>) ODBh.mp4 and ODBz.mp4, respectively [43]. The high energy modes are corresponding to the strong chemical bonds between Si and O atoms [44]. Notably, it can be seen that there are no or only tiny imaginary frequencies near the Γ point, and the structures are therefore expected to be dynamically stable.

3.3. Electronic structure

To examine the electronic structure of oxygen functionalized DB silicene, we first calculate the local DOS (LDOS) for $\text{Si}(\alpha)$, $\text{Si}(\beta)$, and O layers. As shown in figure 3, in both ODB-h and ODB-z, p_z orbital of O atoms contributes to the energy states from -3 eV to -1 eV and hybridizes strongly with p_z orbitals of $\text{Si}(\beta)$. Near the Fermi level $p_{x,y}$ orbitals of O atoms significantly contribute to the electronic structure and hybridize with the p orbitals of $\text{Si}(\alpha)$. The strong hybridization in ODB can decrease the binding energy of O on DB silicene, and thus stabilize the structures. Interestingly, in both cases, the DOS shows a gapless electronic structure with zero DOS at the Fermi level.

Here, we analyze the electronic band structures of honeycomb and zigzag PDB and ODB. As shown in figure 4(a), PDB-h monolayer shows an indirect PBE bandgap of ~ 0.24 eV with valence band maximum (VBM) at K point and conduction band minimum at Γ point, in agreement with the results of previous works [27, 28]. By oxidization, it is found that ODB-h is a gap-less semiconductor where VBM and CBM meeting at the K point. Near Γ point, the local valence band maximum (LVBM) and the local conduction band minimum (LCBM) are at the same place, Γ point, and LVBM degenerates with second local valence band maximum (LVBM-1), which features are also found in PDB-h. The energy difference between LVBM and LCBM at Γ point is about 0.32 eV, 0.27 eV smaller than that in PDB-h. With two bands crossing linearly at the Fermi level, the charge carriers can be characterized by massless Dirac fermions. By a linear

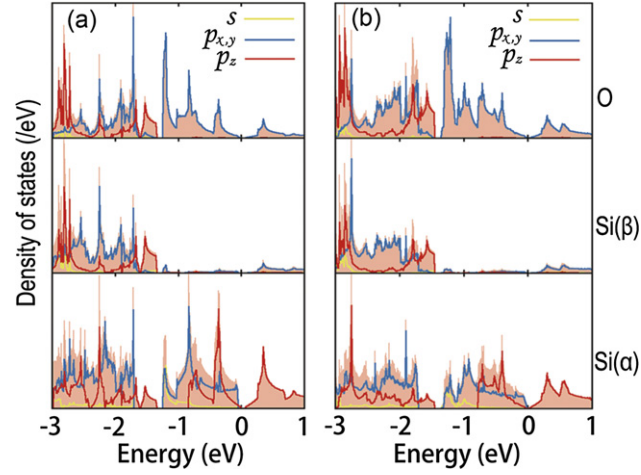


Figure 3. From bottom to top panel is the LDOS projected on Si(α), Si(β), and O layers of (a) ODB-h and (b) ODB-z. PDOS of s , $p_{x,y}$, and p_z orbitals and total DOS of corresponding layers are distinguished with yellow, blue, green lines, and orange area, respectively.

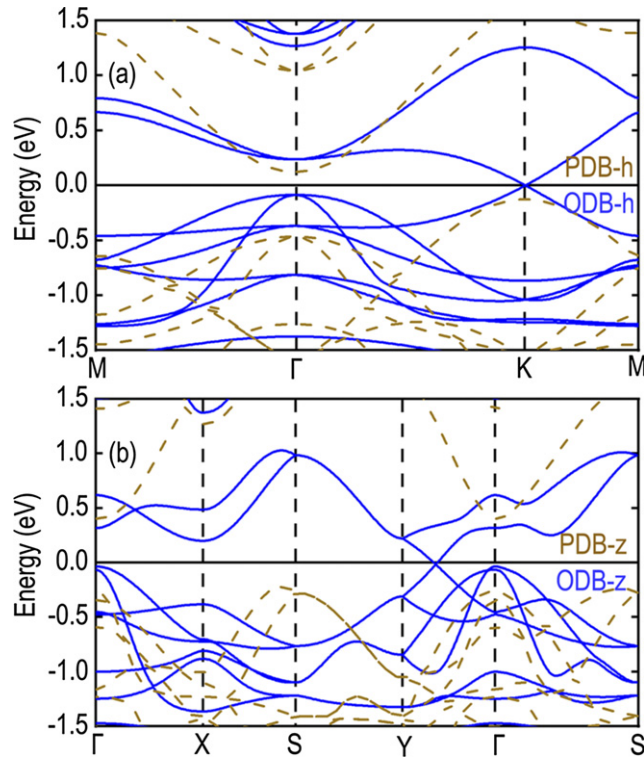


Figure 4. PBE band structure of (a) PDB-h and ODB-h, (b) PDB-z and ODB-z. The energy is set to zero at the Fermi level.

fitting of the band structure, following

$$\nu_F = \frac{1}{\hbar} \nabla_k E(\mathbf{k}), \quad (2)$$

we obtain the Fermi velocity of ODB-h to be $3.1 \times 10^5 \text{ m s}^{-1}$, which is comparable to those of the group IV elemental monolayers ($4.7\text{--}8.5 \times 10^5 \text{ m s}^{-1}$), according to the definition, the effective mass of charge carriers

$$m^* = \hbar \left[\frac{d^2 E(k)}{dk^2} \right] \quad (3)$$

equal to zero near the Fermi level. Therefore, ODB-h silicene is expected to have ultra-high carrier mobility.

As shown in figure 4(b), PDB-z monolayer shows an indirect bandgap of roughly 0.62 eV with CBM both at Γ point and VBM near S point. At the Γ point, the energy level of LVB is only 0.04 eV lower than VBM near S, which is in the correct range for applications in photovoltaics [29]. Interestingly, similar to

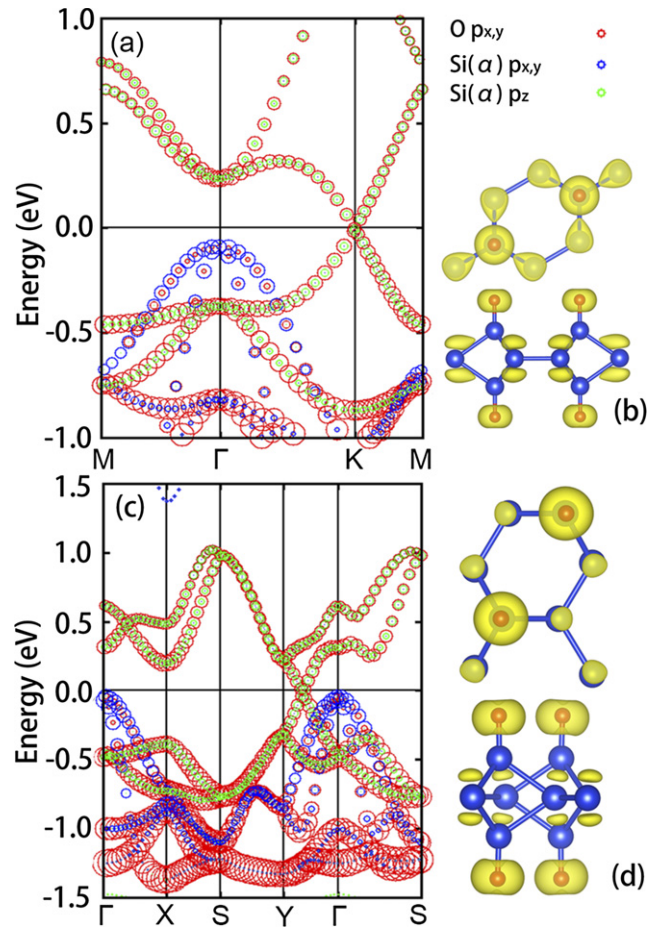


Figure 5. The orbital projected band structures of (a) ODB-h and (b) ODB-z along high symmetry path in the BZ, and the corresponding electronic wave functions of VMB/CBM (c) and (d).

PDB-h silicene, its oxide, ODB-h, is also a gapless semiconductor with two bands crossing linearly at the Fermi level at a point on the path between Y and Γ points. Since the Dirac cone is not situated at high symmetry points, similar to 1T-YN₂ and 1T-LaN₂ [45, 46], H_{4,4,4}-graphyne [47], PAI-graphene [48], and Tungsten boride [49], the Fermi velocities are anisotropic. By a linear fitting of the two bands crossing the Dirac point, we get two different Fermi velocities for the two bands (with slopes $S > 0$ and $S < 0$) $\nu_F(S > 0) = 3.4 \times 10^5 \text{ m s}^{-1}$, and $\nu_F(S < 0) = 2.9 \times 10^5 \text{ m s}^{-1}$. The high Fermi velocity and massless carrier character make the ODB-h and ODB-z ideal materials for building high-speed electronic devices.

As illustrated in figure 3, for ODB-h and ODB-z, the states in the vicinity of the Fermi level are mainly from $p_{x,y}$ orbitals of O atoms, $p_{x,y}$ orbitals of Si(α) atoms and p_z orbitals of Si(α) atoms. To reveal the relationship between electronic band structures and atomic orbitals, we have shown the projected orbitals to bands in figures 5(a) and (c), where the size of a dot demonstrates the contribution of the respective atomic orbital to the electronic bands. It is found that in ODB-h, the LVBM and LVBM-1 at Γ point are dominated by $p_{x,y}$ orbitals of Si(α) with a little contribution by $p_{x,y}$ orbitals of O atoms, while the VBM/CBM at K points is mainly contributed by $p_{x,y}$ orbitals of O atoms, and p_z orbitals of Si(α) atoms. Moreover, in ODB-z, $p_{x,y}$ orbitals of Si(α) atoms mainly contribute to the bands near Γ point, while the Dirac cones are made up by $p_{x,y}$ orbitals of O atoms and p_z orbitals of Si(β) atoms. These features of the bands at K point are also demonstrated in the density profiles of VBM/CBM electronic wave functions shown in figures 5(b) and (d).

3.4. Tight-binding model

To reveal the origin of the Dirac cone explicitly, tight-binding (TB) models are helpful. As illustrated in figures 5(c) and (d), both Si(α) and O atoms contribute to the Dirac cone, the electronic wave functions of O atoms are much larger than those of Si(α) atoms. By proposing simple TB models, which only include the $p_{x,y}$ orbitals of O atoms, we are able to fit the bands near the Fermi level.

To further illustrate the origin of the Dirac points in the two monolayers, we propose two TB models involving the p_x and p_y atomic orbitals. The effective Hamiltonian is taken as in reference [50]

$$H_{\text{TB}} = \sum_{i,\alpha} \varepsilon_i^\alpha c_i^{\alpha+} c_i^\alpha + \sum_{\langle ij \rangle, \alpha, \beta} t_{ij}^{\alpha\beta} (c_i^{\alpha+} c_j^\beta + \text{h.c.}), \quad (4)$$

where ε_i^α , $c_i^{\alpha+}$, and c_i^α represent the on-site energy, creation and annihilation operators of an electron at the α -orbital of the i th atom, respectively. The $t_{ij}^{\alpha\beta}$ parameter is the nearest-neighbour hopping energy of an electron between an α -orbital of i th atom and β -orbital of j th, and $\alpha, \beta \in (p_x, p_y)$. Considering the hexagonal lattice first, we neglect the interactions between the O atoms in different z planes, because the nearest-neighbor distance in the z -direction is more than 20 Å, which is much less than that in the xy plane. We only consider the O atoms in the up/down plane, which is a graphene-like lattice. This graphene-like lattice with $p_{x,y}$ atomic orbitals leads to a Dirac point in the K point, which is similar to in previous investigated systems of BiX/SbX ($X = \text{H, F, Cl, Br, I}$) [51]. According to the TB theory, only one $t_{ij}^{\alpha\beta}$ parameter should be considered, and the hopping energies can be evaluated on the basis of two parameters ($V_{pp\sigma}$ and $V_{pp\pi}$). Since all atoms are oxygen atoms, we can neglect the on-site energy difference of these atoms and set it as 0. Taking $V_{pp\sigma} = 0.4$ eV and $V_{pp\pi} = -0.2$ eV, the band structure from TB calculation can reproduce the DFT band structures close to the Fermi level and the Dirac point in the K point (see figure S1 in the supplementary information (SI)). For the rectangular lattice, we still chose to neglect the interactions between the O atoms in different planes and set the on-site energy to zero. Different from the hexagonal lattice, there are two nearest-neighbour hopping energies, leading to four parameters ($V_{pp\sigma}$, $V_{pp\pi}$, $V'_{pp\sigma}$, and $V'_{pp\pi}$). Taking $V_{pp\sigma} = 0.7$ eV, $V_{pp\pi} = -0.3$ eV, $V'_{pp\sigma} = 0.0$ eV and $V'_{pp\pi} = -0.2$ eV, we obtained the band structure from TB calculations. The location of the Dirac point on the line from Y point to Γ is in good agreement with the result of DFT. From the above TB calculations for the two lattices, we prove that the Dirac points in the two lattices mainly originate from the p_x and p_y atomic orbitals of O atoms.

3.5. Tensile strain

External compressing/tensile strain is reported as a feasible method to tune the electronic structures of 2D materials and transform them between metal, semiconductor, and semimetal [28, 52, 53]. Here we investigate the mechanical and electronic properties of ODB-h and ODB-z under strain, which is applied by changing the lattice constant from a_0 to $(1 + \tau)a_0$. Under biaxial compressing/tensile strains of $-5\% < \tau < 10\%$, as shown in figures 6(a) and (b), the energy changes continuously without any abrupt changes, which indicates that no structural transition occurs. Notably, it does not mean that the two structures are dynamically stable under the strains. Due to the freedom in out-of-plane direction, two-dimensional materials are not dynamically stable under compressive strain [54]. Under tensile strain, as shown in figure S7 in the SI, ODB-h is demonstrated to be still stable when $\tau = 10\%$. In contrast, ODB-z is not dynamically stable when $\tau = 10\%$, but it is stable when $\tau = 8\%$. The structural robustness against intense strain is related to its buckling configuration, similar to the low-buckling structure of silicene.

Under such strains, the Dirac cones near the Fermi level in ODB-h and ODB-z are always conserved. The band structure evolution is presented in the SI (figures S2 and S3). In ODB-h, under tensile strain, the Dirac cone is exactly at the Fermi level, and the bandgap at the Γ point is maintained until $\tau > 9\%$. In contrast, under compressing strain, the Dirac point moves below the Fermi level, and the bandgap at Γ point vanishes for $\tau < -2\%$, making the nanosheets behave as n-type doped. The self-doping behavior arises from the buckling structures, which is also found in LB silicene and germanene [55]. This is because the Dirac cone at K point is dominated by p_z orbitals of Si(α) and $p_{x,y}$ orbitals of O, which are not sensitive to the in-plane strains. In contrast, the LVB and LVB-1 at the Γ point made up of $p_{x,y}$ orbitals of Si(α), which are affected by the change of Si-Si bond length. With similar structural features, ODB-z behaves quite similarly. Under tensile strain, ODB-z preserves the semimetallic property until 9%, while under compressing strain, the self-doping behavior makes it metallic. Overall, for $\tau < 9\%$, the semimetallic features of ODB-h and ODB-z are preserved, with the Fermi velocities changing less than 2.5%, and the insensitivity to tensile strain is advantageous for applications in complicated mechanical environments.

We have also performed band structure calculations with SOC taken into account. Considering that the Si and O are quite light, the SOC effect is generally not strong. For both ODB-h and ODB-z, with or without SOC, the band structures do not change significantly, except that SOC can introduce a bandgap of roughly 10 meV. This bandgap is much more significant than that of LB silicene, i.e. 1.55 meV [5]. The difference is due to the Dirac cone formation mechanism. In LB silicene, the Dirac cone at K point is only formed by p_z orbital of Si atoms, while in ODB-h and ODB-z silicene, $p_{x,y}$ orbitals of O atoms contribute much more than other atomic orbitals.

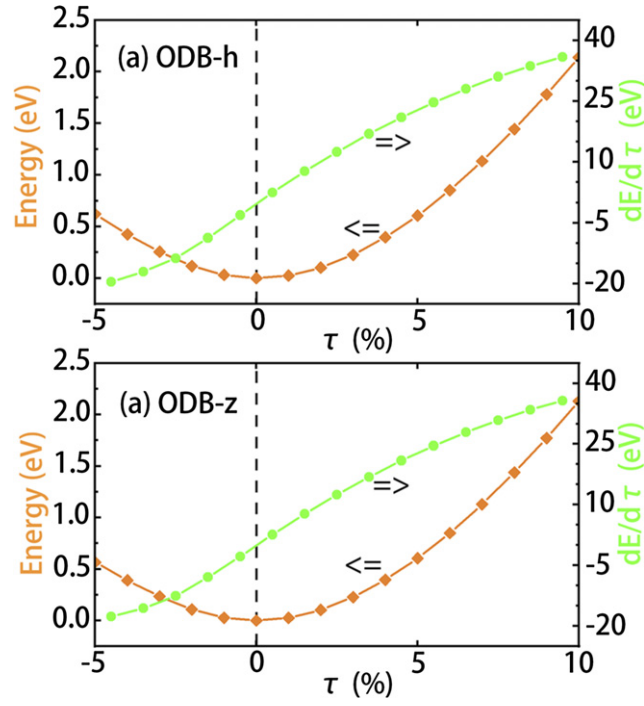


Figure 6. Energy (in orange) and energy derivative (in green) as a function of in-layer tensile strain τ . The energy is set to zero at $\tau = 0$.

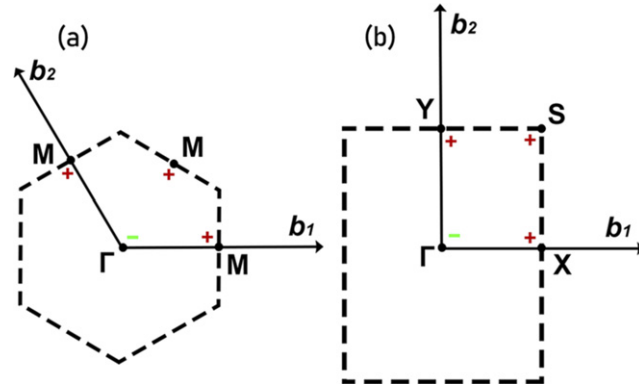


Figure 7. Brillouin zone of (a) ODB-h and (b) ODB-z. b_1 and b_2 are the primitive reciprocal lattice vectors. The signs of δ_i at the time-reversal invariant momenta are labelled as +, -.

Since SOC opens a band gap at the Dirac cones in ODB-h and ODB-z, the topological properties are investigated. It is noteworthy that the chemical adsorption of atoms or molecules also leads to realizing topological insulators [56, 57]. As both ODB-h and ODB-z are inversion symmetric, the topological invariant Z_2 can be calculated using the parity criteria method [58], which claims that the topological invariant can be determined by the parities of the time-reversal and parity invariant points in the BZ, as shown in figure 7. For $2N$ occupied bands, the Z_2 index ν is defined by

$$(-1)^\nu = \prod_i \delta_i, \quad \text{with} \quad \delta_i = \prod_{n=1}^N \xi_{2n}(\Gamma_i), \quad (5)$$

where $\xi_{2n}(\Gamma_i)$ is the parity eigenvalue of the $2n$ th occupied energy band at the time-reversal and parity invariant points Γ_i . For ODB-h, δ_i values of the four time-reversal invariant momenta are -1 at Γ point, and $+1$ at three M points. For ODB-z, the δ_i values are -1 at Γ point, and $+1$ at X , S , and Y points. Thus the Z_2 indexes of ODB-h and ODB-z are nontrivial, e.g. $\nu = 1$, demonstrating that they are both 2D topological insulators.

Considering the underestimation of the bandgap in PBE calculations, we perform HSE06 calculations to examine the results. By HSE06 calculation, in both ODB-h and ODB-z, the electronic bands near the Fermi

level are changed a bit: in most regions, the distance between the lowest conduction bands and highest valence bands is enlarged, while the Dirac cones are preserved. Considering the SOC effect, bandgaps of roughly 20 meV open up at the Dirac cones. These details are shown in figures S5 and S6 in the SI.

4. Conclusions

In summary, based on density functional calculations, we have investigated oxidized form of recently proposed dumbbell silicene DB-h and DB-z and have found that functionalization with O is energetically favorable. We have confirmed the dynamical stability of both oxidized products, 2D ODB-h, and ODB-z silicene by phonon calculations. Although ODB-h and ODB-z have different symmetry, both of them are found to be semimetals with Dirac cones. Also, the semimetallic property is found to be robust against tensile strain up to 9%. Furthermore, their Fermi velocities are as large as $3.1 \times 10^5 \text{ m s}^{-1}$ (in ODB-h) and $2.9\text{--}3.4 \times 10^5 \text{ m s}^{-1}$ (in ODB-z), which are important for application in high-speed electronic devices.

Data availability statement

The data that support the findings of this study are available upon reasonable request from the authors.


Acknowledgments

We thank Mingwen Zhao and Björn Alling for their help and useful discussions. This work is supported by the project Grant (2016-05366) and the Swedish Research Links programme Grant (2017-05447) from the Swedish Research Council, the Fonds voor Wetenschappelijk Onderzoek (FWO-VI), and the FLAG-ERA project TRANS 2D TMD. We gratefully acknowledge supercomputing time allocation by the Swedish National Infrastructure for Computing (SNIC) and PRACE DECI-15 project DYNAMAT. Linyang Li acknowledges financial support from the National Natural Science Foundation of China (Grant No. 12004097), the Natural Science Foundation of Hebei Province (Grant No. A2020202031), and the Foundation for the Introduced Overseas Scholars of Hebei Province (Grant No. C20200313). Xin Chen thanks the China scholarship council for financial support (No. 201606220031).

ORCID iDs

Xin Chen  <https://orcid.org/0000-0002-4120-1138>

Linyang Li  <https://orcid.org/0000-0002-6406-7971>

François M Peeters  <https://orcid.org/0000-0003-3507-8951>

Biplab Sanyal  <https://orcid.org/0000-0002-3687-4223>

References

- [1] Novoselov K S, Geim A K, Morozov S V, Jiang D, Zhang Y, Dubonos S V, Grigorieva I V and Firsov A A 2004 Electric field effect in atomically thin carbon films *Science* **306** 666
- [2] Novoselov K S, Geim A K, Morozov S V, Jiang D, Katsnelson M I, Grigorieva I V, Dubonos S V and Firsov A A 2005 Two-dimensional gas of massless Dirac fermions in graphene *Nature* **438** 197
- [3] Zhang Y, Tan Y-W, Stormer H L and Kim P 2005 Experimental observation of the quantum Hall effect and Berry's phase in graphene *Nature* **438** 201
- [4] Zhu F-f, Chen W-j, Xu Y, Gao C-l, Guan D-d, Liu C-h, Qian D, Zhang S-C and Jia J-f 2015 Epitaxial growth of two-dimensional stanene *Nat. Mater.* **14** 1020
- [5] Vogt P, De Padova P, Quaresima C, Avila J, Frantzeskakis E, Asensio M C, Resta A, Ealet B and Le Lay G 2012 Silicene: compelling experimental evidence for graphenelike two-dimensional silicon *Phys. Rev. Lett.* **108** 155501
- [6] Derivaz M, Dentel D, Stephan R, Hanf M-C, Mehdaoui A, Sonnet P and Pirri C 2015 Continuous germanene layer on Al(111) *Nano Lett.* **15** 2510
- [7] Guzmán-Verri G G and Voon L C L Y 2007 Electronic structure of silicon-based nanostructures *Phys. Rev. B* **76** 075131
- [8] Cahangirov S, Topsakal M, Aktürk E, Şahin H and Ciraci S 2009 Two- and one-dimensional honeycomb structures of silicon and germanium *Phys. Rev. Lett.* **102** 236804
- [9] Liu C C, Feng W and Yao Y 2011 Quantum spin Hall effect in silicene and two-dimensional germanium *Phys. Rev. Lett.* **107** 076802
- [10] Lalmi B, Oughaddou H, Enriquez H, Kara A, Vizzini S, Ealet B and Aufray B 2010 Epitaxial growth of a silicene sheet *Appl. Phys. Lett.* **97** 223109
- [11] Kara A, Enriquez H, Seitsonen A P, Voon L C L Y, Vizzini S, Aufray B and Oughaddou H 2012 A review on silicene - new candidate for electronics *Surf. Sci. Rep.* **67** 1
- [12] Fleurence A, Friedlein R, Ozaki T, Kawai H, Wang Y and Yamada-Takamura Y 2012 Experimental evidence for epitaxial silicene on diboride thin films *Phys. Rev. Lett.* **108** 245501

- [13] Feng B, Ding Z, Meng S, Yao Y, He X, Cheng P, Chen L and Wu K 2012 Evidence of silicene in honeycomb structures of silicon on Ag(111) *Nano Lett.* **12** 3507
- [14] Li G *et al* 2018 Stable silicene in graphene/silicene van der Waals heterostructures *Adv. Mater.* **30** 1804650
- [15] Jose D and Datta A 2014 Structures and chemical properties of silicene: unlike graphene *Acc. Chem. Res.* **47** 593
- [16] Krawiec M 2018 Functionalization of group-14 two-dimensional materials *J. Phys. Condens. Matter* **30** 233003
- [17] Molle A, Grazianetti C, Tao L, Taneja D, Alam M H and Akinwande D 2018 Silicene, silicene derivatives, and their device applications *Chem. Soc. Rev.* **47** 6370
- [18] Qiu J, Fu H, Xu Y, Zhou Q, Meng S, Li H, Chen L and Wu K 2015 From silicene to half-silicane by hydrogenation *ACS Nano* **9** 11192
- [19] Wei W, Dai Y and Huang B 2017 Hydrogenation of silicene on Ag(111) and formation of half-silicane *J. Mater. Chem. A* **5** 18128
- [20] Nguyen M-T, Phong P N and Tuyen N D 2015 Hydrogenated graphene and hydrogenated silicene: computational insights *ChemPhysChem* **16** 1733
- [21] Xu Y, Yan B, Zhang H J, Wang J, Xu G, Tang P, Duan W and Zhang S C 2013 Large-gap quantum spin Hall insulators in tin films *Phys. Rev. Lett.* **111** 136804
- [22] Lin X and Ni J 2012 Much stronger binding of metal adatoms to silicene than to graphene: a first-principles study *Phys. Rev. B* **86** 75440
- [23] De Padova P, Quaresima C, Olivieri B, Perfetti P and Le Lay G 2011 Strong resistance of silicene nanoribbons towards oxidation *J. Phys. D: Appl. Phys.* **44** 312001
- [24] Molle A, Grazianetti C, Chiappe D, Cinquanta E, Cianci E, Tallarida G and Fanciulli M 2013 Hindering the oxidation of silicene with non-reactive encapsulation *Adv. Funct. Mater.* **23** 4340
- [25] Zaminpayma E and Nayebe P 2016 Band gap engineering in silicene: a theoretical study of density functional tight-binding theory *Phys. E* **84** 555
- [26] Özçelik V O and Ciraci S 2013 Local reconstructions of silicene induced by adatoms *J. Phys. Chem C* **117** 26305
- [27] Cahangirov S, Özçelik V O, Xian L, Avila J, Cho S, Asensio M C, Ciraci S and Rubio A 2014 Atomic structure of the 3×3 phase of silicene on Ag(111) *Phys. Rev. B* **90** 35448
- [28] Zhang T, Zeng Z-Y, Cheng Y, Chen X-R and Cai L-C 2016 Dumbbell silicene: a strain-induced room temperature quantum spin Hall insulator *New J. Phys.* **18** 043001
- [29] Borlido P, Rödl C, Marques M A L and Botti S 2018 The ground state of two-dimensional silicon *2D Mater.* **5** 035010
- [30] Chen X, Li L and Zhao M 2015 Dumbbell stanane: a large-gap quantum spin hall insulator *Phys. Chem. Chem. Phys.* **17** 16624
- [31] Wang Y-p, Ji W-x, Zhang C-w, Li P, Li F, Wang P-j, Li S-s and Yan S-s 2016 Large-gap quantum spin Hall state in functionalized dumbbell stanene *Appl. Phys. Lett.* **108** 073104
- [32] Ding Y and Wang Y 2018 Tunable electronic structures of hydrogenated zigzag and armchair dumbbell silicene nanosheets: a computational study *J. Phys. Chem C* **122** 2
- [33] Kresse G and Joubert D 1999 From ultrasoft pseudopotentials to the projector augmented-wave method *Phys. Rev. B* **59** 1758
- [34] Blöchl P E 1994 Projector augmented-wave method *Phys. Rev. B* **50** 17953
- [35] Kresse G and Hafner J 1993 *Ab initio* molecular dynamics for liquid metals *Phys. Rev. B* **47** 558
- [36] Kresse G and Furthmüller J 1996 Efficient iterative schemes for *ab initio* total-energy calculations using a plane-wave basis set *Phys. Rev. B* **54** 11169
- [37] Perdew J P, Burke K and Ernzerhof M 1996 Generalized gradient approximation made simple *Phys. Rev. Lett.* **77** 3865
- [38] Hobbs D, Kresse G and Hafner J 2000 Fully unconstrained noncollinear magnetism within the projector augmented-wave method *Phys. Rev. B* **62** 11556
- [39] Parlinski K, Li Z Q and Kawazoe Y 1997 First-principles determination of the soft mode in Cubic ZrO_2 *Phys. Rev. Lett.* **78** 4063
- [40] Togo A, Oba F and Tanaka I 2008 First-principles calculations of the ferroelastic transition between rutile-type and CaCl_2 -type SiO_2 at high pressures *Phys. Rev. B* **78** 134106
- [41] Krukau A V, Vydrov O A, Izmaylov A F and Scuseria G E 2006 Rationale for mixing exact exchange with density functional approximations *J. Chem. Phys.* **125** 6158
- [42] Kageshima H and Shiraishi K 1997 Microscopic mechanism for SiO_2/Si interface passivation: $\text{Si}=\text{O}$ double bond formation *Surf. Sci.* **380** 61
- [43] Miranda H 2015 Phonon visualization website <https://henriquemiranda.github.io/phononwebsite/>
- [44] Eckert J 1984 High energy phonons: overview **540–547** *LA-10227-C-Vol2*
- [45] Kong X, Li L, Leenaerts O, Wang W, Liu X-J and Peeters F M 2018 Quantum anomalous Hall effect in a stable 1T- YN_2 monolayer with a large nontrivial bandgap and a high Chern number *Nanoscale* **10** 8153
- [46] Li L, Kong X, Chen X, Li J, Sanyal B and Peeters F M 2020 Monolayer 1t-lan2: Dirac spin-gapless semiconductor of p-state and Chern insulator with a high Chern number *Appl. Phys. Lett.* **117** 143101
- [47] Li L, Kong X and Peeters F M 2019 New nanoporous graphyne monolayer as nodal line semimetal: double Dirac points with an ultrahigh fermi velocity *Carbon* **141** 712–8
- [48] Chen X, Bouhon A, Li L, Peeters F M and Sanyal B 2020 Pai-graphene: a new topological semimetallic two-dimensional carbon allotrope with highly tunable anisotropic Dirac cones *Carbon* **170** 477–86
- [49] Wang A, Shen L, Zhao M, Wang J, Zhou W, Li W, Feng Y and Liu H 2019 Tungsten boride: a 2d multiple Dirac semimetal for the hydrogen evolution reaction *J. Mater. Chem. C* **7** 8868–73
- [50] Zhao M, Zhang X and Li L 2015 Strain-driven band inversion and topological aspects in antimonene *Sci. Rep.* **5** 16108
- [51] Song Z *et al* 2014 Quantum spin Hall insulators and quantum valley Hall insulators of BiX/SbX ($X = \text{H}, \text{F}, \text{Cl}$ and Br) monolayers with a record bulk band gap *NPG Asia Mater.* **6** 147
- [52] Zhao M, Chen X, Li L and Zhang X 2015 Driving a GaAs film to a large-gap topological insulator by tensile strain *Sci. Rep.* **5** 8441
- [53] Zhao M, Zhang X and Li L 2015 Strain-driven band inversion and topological aspects in antimonene *Sci. Rep.* **5** 16108
- [54] Frank O, Tsoukleri G, Parthenios J, Papagelis K, Riaz I, Jalil R, Novoselov K S and Galiotis C 2010 Compression behavior of single-layer graphenes *ACS Nano* **4** 3131–8
- [55] Wang Y and Ding Y 2013 Strain-induced self-doping in silicene and germanene from first-principles *Solid State Commun.* **155** 6
- [56] Li S-s, Ji W-x, Hu S-j, Zhang C-w and Yan S-s 2017 Effect of amidogen functionalization on quantum spin hall effect in $\text{Bi}/\text{Sb}(111)$ films *ACS Appl. Mater. Interfaces* **9** 41443–53
- [57] Wang Y-p, Ji W-x, Zhang C-w, Li P, Zhang S-f, Wang P-j, Li S-s and Yan S-s 2017 Two-dimensional arsenene oxide: a realistic large-gap quantum spin hall insulator *Appl. Phys. Lett.* **110** 213101
- [58] Fu L and Kane C L 2007 Topological insulators with inversion symmetry *Phys. Rev. B* **76** 045302